nature communications

Article

https://doi.org/10.1038/s41467-024-55159-0

# Gigantic Tellegen responses in metamaterials

Received: 21 July 2024

Accepted: 3 December 2024

Published online: 02 January 2025

Check for updates

Qingdong Yang[1,4], Xinhua Wen[1,4], Zhongfu Li[1,4], Oubo You[1] & Shuang Zhang[1,2,3]

Tellegen medium has long been a topic of debate, with its existence being contested over several decades. It was first proposed by Tellegen in 1948 and is characterized by a real-valued cross coupling between electric and magnetic responses, distinguishing it from the well-known chiral medium that has imaginary coupling coefficients. Significantly, Tellegen responses are closely linked to axion dynamics, an extensively studied subject in condensed matter physics. Here, we report the realization of Tellegen metamaterials in the microwave region through a judicious combination of subwavelength metallic resonators, gyromagnetic materials, and permanent magnets. We observe the key signature of the Tellegen response – a Kerr rotation for reflected wave, while the polarization remains the same in the transmission direction. The retrieved effective Tellegen parameter is several orders of magnitude greater than that of natural materials. Our work opens door to a variety of non-reciprocal photonic devices and may provide a platform for studying axion physics.

Tellegen media, characterized by a real-valued cross-coupling between electric and magnetic responses, are first theoretically proposed by Tellegen in 1948 for designing an electromagnetic gyrator[1]. Ever since then, Tellegen media has drawn significant attention and sparked extensive discussions regarding its existence in electromagnetics[2–7]. The Tellegen coupling, as a subclass of the bianisotropic coupling, renders additional degrees of freedom for manipulating the light-matter interactions and controlling the wave polarization[8,9]. When an electromagnetic wave interacts with a Tellegen material, angular momentum is transferred to reflected waves, inducing a rotation of the polarization plane of the reflected wave, referred to as the Kerr effect[10]. Differing from extensively studied reciprocal chiral media[11–13], Tellegen media possess a nonreciprocal nature due to the broken parity symmetry and time-reversal symmetry. Therefore, Tellegen materials offer the promise of nonreciprocal wave propagation, with practical applications such as electromagnetic isolators and nonreciprocal twist polarizers[14,15]. In addition, the Tellegen response is closely associated with axion electrodynamics, which has drawn great attention due to its connections with topological insulators, high-energy physics, and dark matters[16–19]. Although axion response has been extensively studied in condensed matter physics[20,21] and has been experimentally reported in some antiferromagnetic crystals[22] and electronic topological insulators[18,23–27], the experimental realization of a strong and flexibly tunable axion response has remained elusive. Interestingly, the electrodynamic equations of a media with a pure Tellegen response have the same form as those of the axion media[28–30], making it an exciting opportunity to explore axion-related physics with Tellegen materials. Despite the substantial interest and significance of the Tellegen response in both applied and fundamental physics, most of the research about the Tellegen response has remained confined to theoretical exploration over the past two decades[22,31–35]. A ferrite-based structure has been proposed as a Tellegen particle in the microwave regime, based on the measurement of the amplitude of the cross-polarized wave in a waveguide[36,37]. However, it was later argued that such a measurement in the waveguide was not convincing, as no definite and stable polarizability parameters characterizing the

[1]New Cornerstone Science Laboratory, Department of Physics, University of Hong Kong, 999077 Hong Kong, China. [2]Department of Electrical & Electronic Engineering, University of Hong Kong, 999077 Hong Kong, China. [3]Materials Innovation Institute for Life Sciences and Energy (MILES), HKU-SIRI, 518000 Shenzhen, China. [4]These authors contributed equally: Qingdong Yang, Xinhua Wen, Zhongfu Li. e-mail: shuzhang@hku.hk

magnetoelectric properties could be found[31]. To date, a decisive demonstration of Tellegen media exhibiting their key features still remains elusive.

In this work, we report the experimental realization of a metamaterial with a pure Tellegen response, and the first observation of a gigantic Tellegen response that is several orders of magnitude stronger than that observed in natural materials. Specifically, combining gyromagnetic materials and split-ring resonators, a Tellegen metamaterial with in-phase magnetoelectric coupling is designed and fabricated. When an electromagnetic wave impinges on the Tellegen metamaterial slab, the polarization of the reflection wave is rotated (i.e., the Kerr effect), while the transmission wave remains the same polarization as the incident field, serving as the most key characteristics of a pure Tellegen response that has been missing so far. Notably, giant Kerr rotation reaching 90° is observed, indicating a strong effective Tellegen coupling parameter several orders of magnitude greater than that of intrinsic magnetoelectric materials (e.g., $Cr_2O_3$[22]). It is noted that the pure Tellegen response is closely associated with axion electrodynamics. Furthermore, the measured magnetoelectric nearfield distribution within a metamaterial unit-cell provides more evidence supporting the rotation of polarization response in the far-field. The experimental realization of Tellegen metamaterials not only holds promise for various practical applications, such as electromagnetic isolators and nonreciprocal twist polarizers, but also opens up significant opportunities for the experimental exploration novel concepts related to axion electrodynamics in microwave range[38].

## Results

### Tellegen media's polarizability properties

We start with a general description of the polarizability of bianisotropic meta-atoms, which plays a pivotal role in governing the electromagnetic response of bianisotropic metamaterials. For a general bianisotropic meta-atom, the induced electric dipole moments **p** and magnetic dipole moments **m** can be related to the incident electromagnetic fields $\mathbf{E}_{in}$ and $\mathbf{H}_{in}$ by a polarizability tensor[3,39]:

$$\begin{pmatrix} \mathbf{p} \\ \mathbf{m} \end{pmatrix} = \begin{pmatrix} \overline{\overline{\alpha}}_{ee} & \overline{\overline{\alpha}}_{em} \\ \overline{\overline{\alpha}}_{me} & \overline{\overline{\alpha}}_{mm} \end{pmatrix} \begin{pmatrix} \mathbf{E}_{in} \\ \mathbf{H}_{in} \end{pmatrix}, \tag{1}$$

where $\overline{\overline{\alpha}}_{ee}$ and $\overline{\overline{\alpha}}_{mm}$ denote the electric and magnetic polarizability tensors respectively; $\overline{\overline{\alpha}}_{em}$ and $\overline{\overline{\alpha}}_{me}$ respectively represent the electromagnetic and magnetoelectric polarizability tensors, describing the cross-coupling between the electric and magnetic responses. For the metamaterial with isotropic in-plane response, the bianisotropic coupling can be categorized into four basic classes—two that are reciprocal (chiral and omega), and two that are nonreciprocal (Tellegen and moving)[40,41]. Each category exhibits unique transmission and reflection in response to incident waves, determined by the phase and polarization of induced dipoles[42–44]. Tellegen materials represents a specific class of bianisotropic coupling that is characterized by a real-valued (in-phase) cross-coupling polarizability.

To gain a comprehensive understanding of Tellegen response, we provide a comparative illustration depicting the electromagnetic response between a Tellegen metamaterial slab and an extensively studied chiral metamaterial slab in Fig. 1[45–47]. We assume that the metamaterial slabs are positioned in the $x$-$y$ plane, and they are illuminated by a normally incident $y$-polarized plane wave. For a chiral meta-atom characterized by an imaginary-valued cross-coupling polarizability, the electric field $E_y$ (magnetic field $H_x$) induces a magnetic dipole $-im_y$ (an electric dipole $ip_x$), as illustrated in the left inset of Fig. 1a. Notably, the presence of the imaginary unit $i$ indicates that the induced magnetic and electric dipole moments exhibit an additional $\pi/2$ phase shift with respect to incident fields. In the chiral composite slab, the two dipole moments both emit scattered waves of orthogonal polarization to that of incident wave, which constructively interference in the forward direction, giving rise to a rotation in the polarization of the transmitted wave. Consequently, as depicted in Fig. 1a, the incident wave, polarized along the $y$-axis, transforms into a linear polarized transmitted wave, while the polarization plane of the reflected wave remains unchanged due to the destructive interference of the $x$-polarized scattered wave.

In contrast, in the case of a Tellegen meta-atom, the induced magnetic (electric) dipole moments align parallel to the incident electric (magnetic) field (the right inset of Fig. 1b) with an in-phase coupling. It is worth noting that the metamaterials under investigation exhibit an isotropic response only in the $x$-$y$ plane, while the electromagnetic response in the $z$-direction is different. In the metamaterial slab with pure Tellegen response, the effective electromagnetic response can be expressed as the following constitutive equations[48]:

$$\begin{pmatrix} D_x \\ D_y \end{pmatrix} = \varepsilon_0 \varepsilon \begin{pmatrix} E_x \\ E_y \end{pmatrix} + \frac{1}{c_0} \begin{pmatrix} \xi & 0 \\ 0 & \xi \end{pmatrix} \begin{pmatrix} H_x \\ H_y \end{pmatrix},$$

$$\begin{pmatrix} B_x \\ B_y \end{pmatrix} = \mu_0 \mu \begin{pmatrix} H_x \\ H_y \end{pmatrix} + \frac{1}{c_0} \begin{pmatrix} \xi & 0 \\ 0 & \xi \end{pmatrix} \begin{pmatrix} E_x \\ E_y \end{pmatrix} \tag{2}$$

where $\varepsilon$ and $\mu$ are the effective permittivity and permeability, and $\xi$ represents the effective Tellegen parameter. The Tellegen response, featuring a real-valued cross-coupling term, violates reciprocity while holding the Hermitian requirements that the induced magnetic dipole $m_y$ and electric dipole $p_x$ have the same phase as the incident fields. In contrast to the chiral slabs, scattered waves of orthogonal polarization interfere constructively (destructively) in the backward (forward) direction, resulting in a rotation of the polarization plane of the reflected wave. This effect is called the Kerr effect. It should be noted that the metamaterial slab with pure Tellegen response exhibits the Kerr effect for arbitrary polarization of linearly polarized incident waves and ensures that the transmitted wave passing through the Tellegen metamaterial slab retains the same polarization as the incident wave as schematically illustrated in Fig. 1b.

Interestingly, the constitutive relations of the Tellegen media in Eq. (2) can be rewritten as:

$$\boldsymbol{H} = \frac{\boldsymbol{B}}{\mu_0 \mu} - \alpha \vartheta \boldsymbol{E} \tag{3}$$

$$\boldsymbol{D} = \varepsilon_0 \varepsilon' \boldsymbol{E} + \alpha \vartheta \boldsymbol{B},$$

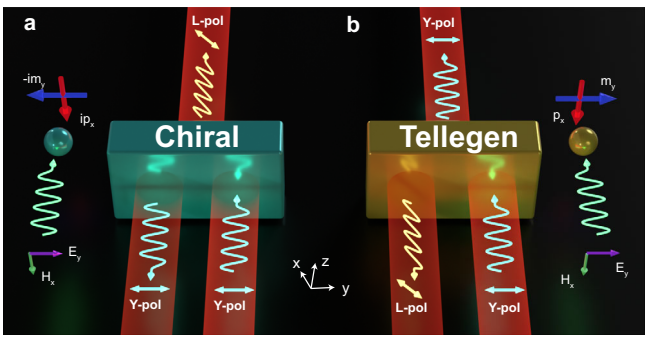


**Fig. 1 | Principle of chiral and Tellegen response.** Schematics of the electromagnetic response of (**a**) a chiral and (**b**) a Tellegen metamaterial slab. The insets adjacent to each schematic display the cross-coupling polarizability of a chiral meta-atom (green sphere) and a Tellegen meta-atom (brown sphere), respectively. Here only dipole moments resulted from the cross-coupling are shown for clarity. The metamaterial slabs positioned in the $x$-$y$ plane, are subjected to normal illumination by a plane wave propagating along the $z$-direction. The labels "Y-pol" and "L-pol" correspond to $y$-polarization and linear polarization, respectively.

https://doi.org/10.1038/s41467-024-55159-0

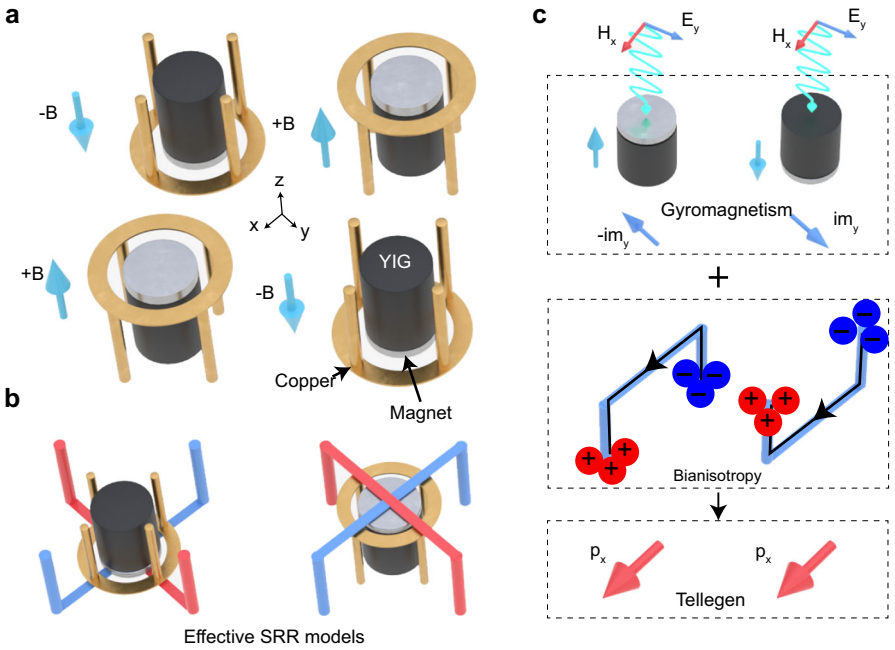


**Fig. 2 | The design of the metamaterial unit-cell with the pure Tellegen response. a** Schematic of a Tellegen unit-cell comprised four sub-particles that are constructed by inserting an YIG rod (black cylinder) and a magnet (silvery cylinder) in the saddle-shaped metallic coil (yellow color). Two sub-particles invert the orientation, biased by opposite external magnetic fields, as denoted by blue arrows. **b** The saddle-shaped metallic coil of the sub-particles can be effectively regarded as two orthogonal SRRs along *x*-direction (blue color) and *y*-direction (red color), respectively. **c** The underlying mechanism responsible for generating the pure Tellegen response. Upon the incidence of a plane wave with *y*-polarization, the *x*-oriented magnetic field $H_x$ induces a magnetic dipole $-im_y$ in the YIG rod, and then excites the electric current along the SRR in the *x*-direction, inducing the electric dipole $p_x$. The current and charge accumulation are shown in the SRR. The inversed structure cancels the unwanted gyromagnetic and bianisotropic response.

where the field vectors $\boldsymbol{B}, \boldsymbol{H}, \boldsymbol{D}, \boldsymbol{E}$ contain both *x* and *y* components. α is coupling constant. Equation (3) presents the constitutive relations of the axion media[28,49]. The axion-coupling term $\vartheta$ is related to the Tellegen coupling term by $\alpha\vartheta = \xi/c_0\mu_0\mu$. The effective permittivity of the axion media is modified as $\varepsilon_0\varepsilon' = \varepsilon_0\varepsilon - \xi^2/c_0^2\mu_0\mu$, while the effective permeability remains the same as that of the Tellegen media. The presence of the axion-coupling term modifies the Maxwell equations within axion media, giving an additional term in Lagrangian density (Supplementary Materials Sec. 1). Consequently, the Tellegen metamaterial, which embodies the equations of axion electrodynamics, serves as a practical platform for investigating the intriguing associated phenomena. In particular, at the interface between the air and Tellegen metamaterial slab, the sudden change of the axion field affects the electromagnetic response, giving rise to the distinctive Kerr effect, which is the fingerprint of the axion response[18].

## Tellegen metamaterial design

To achieve pure Tellegen coupling as described in Eq. (2), we propose a Tellegen metamaterial design that incorporates saddle-shaped connective metallic coils and rods of gyromagnetic materials biased by external magnetic fields generated by locally positioned magnets, as schematically shown in Fig. 2a. Specifically, each sub-unit consists of an Yttrium-iron-garnet (YIG) rod (black cylinder) placed in the center of the saddle-shaped connective metallic coil (yellow color), biased by a small magnet (bright disc). The saddle-shaped metallic coils strongly confine the magnetic field, such that the incident wave can efficiently interacts with the YIG rod which is commonly utilized to achieve nonreciprocal response[50,51]. This, in turn, enables the generation of a strong cross-coupling response. Each unit-cell comprises four sub-units, with two of them biased by opposite external magnetic fields relative to the other two, as indicated by the blue arrows in Fig. 2a. We note that such a metamaterial unit-cell shares some similarities with a recent theoretical work (ref. 33.) in terms of the structural configuration. The saddle-shaped connective metallic coils, with four-fold rotational symmetry, can be effectively regarded as two orthogonal splitting resonator rings (SRRs), which are represented by red and blue metal strips, respectively, as shown in Fig. 2b. Similarly, the inverted sub-particle corresponds to flipped SRRs, as shown in the right panel of Fig. 2b.

The schematic in Fig. 2c elucidates the underlying mechanism responsible for generating the pure Tellegen response within the unit-cell in Fig. 2a. When a plane wave with *y*-polarization is incident onto the sub-unit structure, the *x*-oriented magnetic field $H_x$ induces an oscillating magnetic dipole moment $-im_y$ (upper panel), due to the gyromagnetic effect (i.e., the antisymmetric part of the YIG permeability tensor). This magnetic dipole is orthogonal to incident field, which effectively rotates the incident field by 90 degrees. According to the Lenz-Faraday law, the magnetic dipole moment excites the electric current in the SRR and causes opposite charge accumulation in the two vertical arms, leading to an *x*-directed electric dipole $p_x$ (lower panel). The induced electric dipole is collinear with the incident magnetic field, representing an in-phase cross-coupling, which is the essence of the Tellegen response. As depicted in Fig. 2c, the sub-units, biased by opposite magnetic fields, induce magnetic dipole moments of opposite polarities (denoted by $-im_y$ and $im_y$ respectively), while giving rise to the same electric dipoles $p_x$. The *y*-oriented electrical field $E_y$ induce $m_y$ in a similar manner, as shown in Supplementary Fig. 1. Consequently, the metamaterial unit-cell, consisting of two sets of sub-units with reversed orientation, effectively cancels out unwanted responses such as the gyromagnetic and omega response. We numerically calculate the magnetic and electric dipole moments, validating the pure Tellegen response of the metamaterial (refer to Supplementary Materials Sec. 2 for more details). In addition, the microscopic polarizability analysis of the metamaterial unit-cell is in concordance with the results of the structural symmetry analysis (refer to Supplementary

https://doi.org/10.1038/s41467-024-55159-0

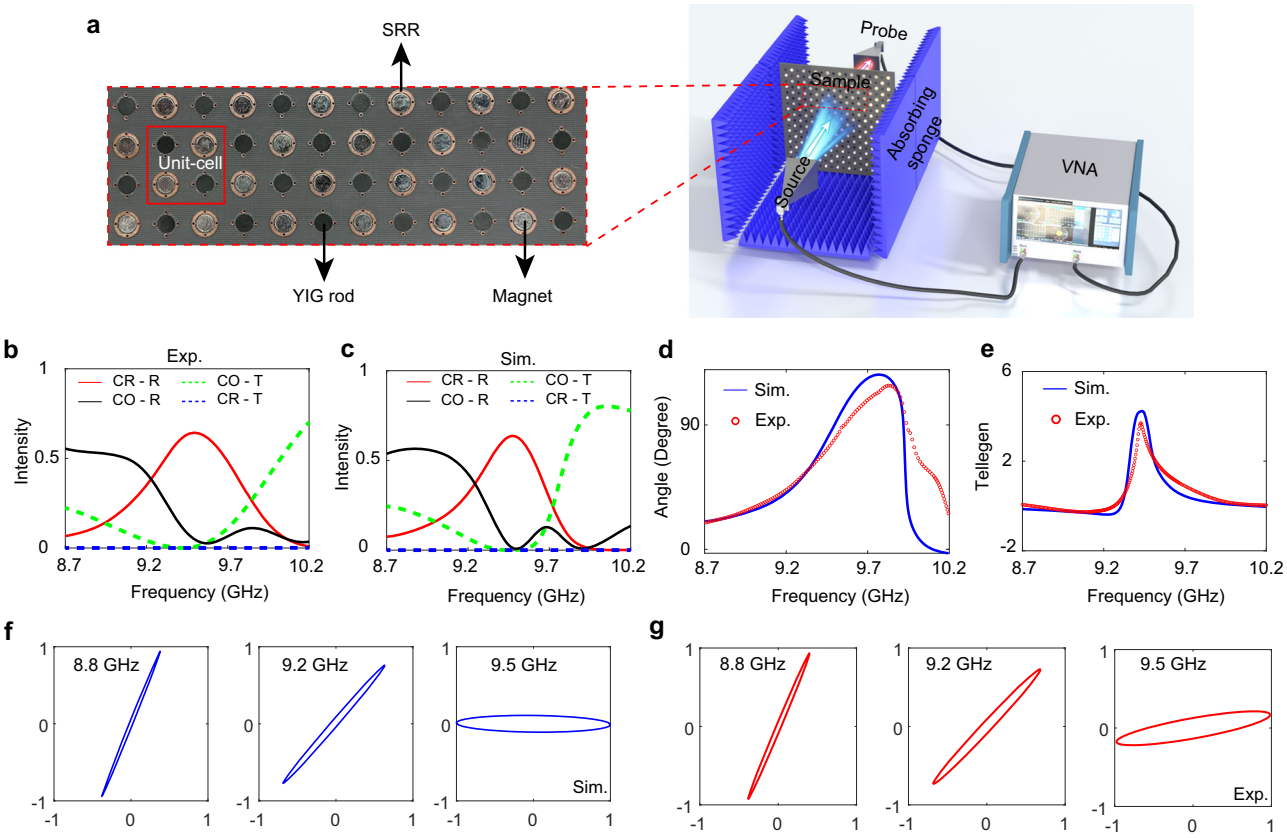


**Fig. 3 | Experimental measurement of the Tellegen slab. a** The experimental setup for measuring the transmission, utilizing antennas connected to a VNA. The left panel displays a zoom-out portion of the actual sample, with the silver and black cylinders representing the magnets and YIG rods inserted into the circuit board, respectively. The red frame highlights a unit-cell structure. **b**, **c** Measured and simulated reflection and transmission intensity spectra. The labels "CO-" and "CR-" indicate co-polarization and cross-polarization respectively, and "T" and "R" present transmission and reflection respectively. **d** Simulated (lines) and measured (circles) Kerr rotation angle induced by the Tellegen response. **e** Extracted effective Tellegen parameter obtained from simulated (line) and measured (circles) results. **f**, **g** The simulated and measured polarization state of the reflected beam at the specific frequencies.

Materials Sec. 3 for details), both indicating the achievement of a pure and isotropic Tellegen response in the *x*-*y* plane.

## Experiment measurement

A Tellegen metamaterial slab is constructed by arranging the designed metamaterial unit-cell structure periodically along the *x*- and *y*-directions with a period of $L = 17.6$ mm. The sample was fabricated using the Printed Circuit Board (PCB) technology. The saddle-shaped connective metallic coil is embedded inside Teflon with a relative permittivity of 2.72 and loss tangent of 0.008. The YIG rods and permanent magnets are inserted into the circular apertures drilled into the fabricated circuit board, as shown in the photograph presented in the left panel of Fig. 3a. The red frame marks the actual unit-cell structure, wherein the permanent magnets of two sub-particles have reversed orientation to provide opposite magnetic bias. For the experimental measurement of the transmission, the sample is positioned between two linearly polarized wideband horn antennas connected to the ports of a Vector Network Analyzer (VNA), as shown in Fig. 3a. The incident wave from the source horn antenna is polarized in the *y*-direction and normally impinged on the metamaterial slab. By aligning the receiving antenna parallel (perpendicular) to the source antenna, we can measure the co-polarized (cross-polarized) transmission signals. Similarly, by placing the probe antenna on the same side as the source antenna, we can measure both co- and cross-polarized reflected signals. More details about the sample are provided in the Supplementary Materials Sec. 4.

The measured reflection and transmission intensity spectra for both the co- and cross-polarization are shown in Fig. 3b. The reflection spectra reveal that the reflection wave undergoes polarization rotation across a broad frequency range, indicating the presence of the Kerr effect induced by the Tellegen response. At the resonant frequency of 9.5 GHz, the cross-polarized reflectivity reaches its maximum, while the co-polarized reflectivity is almost zero, representing a near-complete cross polarization conversion in reflection. This indicates a strong Tellegen response at the resonance frequency. Furthermore, as shown by Fig. 3b, the transmission wave remains the same polarization as the incident wave, as evidenced by the near-zero cross-polarization transmissivity observed across the entire frequency range of interest, which is another key signature of a pure Tellegen response. We also perform simulation on the reflection and transmission, with the results shown in Fig. 3c. The simulation is conducted using the commercial software COMSOL Multiphysics, employing a periodic unit-cell structure. Despite some discrepancies in the higher frequency range may be caused by the inhomogeneous distribution of the static magnetic field in the experiment, the simulation results show good agreement with the measured spectra, further validating the presence of pure Tellegen response of the metamaterial slab.

Both the simulated and measured polarization rotation of reflected light are provided in Fig. 3d, which confirm the rotation of the reflected light across a wide range of frequencies. The simulated and measured polarization states of the reflected beam at the specific frequencies are shown in Figs. 3f, g. Due to the presence of loss in the real structure, the polarization state of the reflected beam slightly deviates from the linear polarization and become elliptically polarized. When the loss is excluded from the simulation model, the reflected

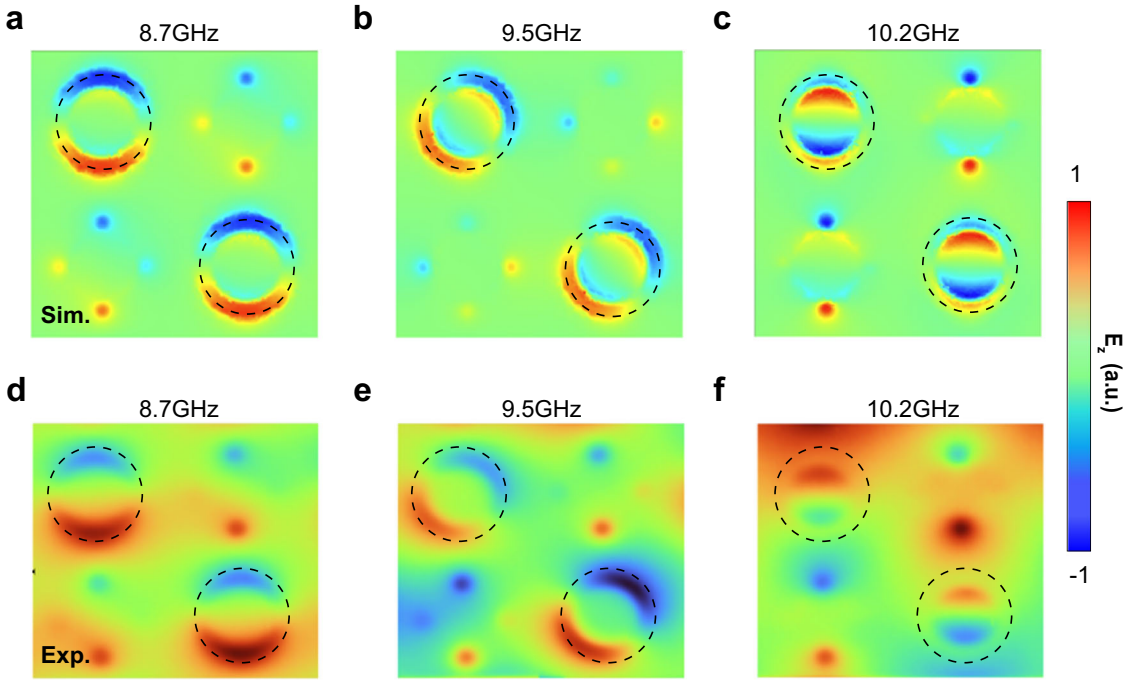


**Fig. 4 | Near-field characterization of the Tellegen metamaterial slab.** The simulated (**a**–**c**) and measured (**d**–**f**) $E_z$ component of the nearfield for a metamaterial unit-cell at three different frequencies: 8.7 GHz, 9.5 GHz, and 10.2 GHz. The center of the circular metal coil is plotted by dashed line.

wave exhibits linear polarization, as demonstrated in Supplementary Fig. 6. Nonetheless, one can still use the major axis to characterize the polarization rotation, as explained in detail in Supplementary Materials Sec. 5. Near the reflectivity peak at 9.5 GHz, the Kerr rotation is approximately 90° for both simulation and measurement, confirming a near-complete cross polarization conversion from *y*-polarized incident wave to *x*-polarized reflected wave. The rotation angle reaches maximum at a slightly higher frequency than the resonance for both the simulation and experiment. The measured rotation angle is much larger than that of intrinsic magnetoelectric materials such as $Cr_2O_3$.

The polarization rotation angle of reflected light is closely related to the Tellegen coupling parameters[52]:

$$\tan\theta_{\mathrm{Kerr}} = \frac{2\xi}{\varepsilon - \mu} \tag{4}$$

Notably, the induced Kerr rotation $\theta_{Kerr}$ is independent of the thickness of the metamaterial slab. For our metamaterial with isotropic in-plane response, effective medium description is valid for the *z*-direction, which is supported by consistent simulated Tellegen parameters extracted from the metamaterials of multiple layers (see Supplementary Fig. 7). Consequently, the effective Tellegen parameter can be retrieved from the transmission and reflectance, as shown in Fig. 3e. The retrieved parameter from both the experimental and simulation results reach its peak at the resonance frequency. Around the resonance frequency, the measured Tellegen parameter $\xi$ is approximately 3.5, several orders of magnitude greater than that of $Cr_2O_3$. Such a substantial Tellegen coupling can be attributed to the engineered resonance of the metamaterial which significantly increases the interaction between the SRR and the YIG rod. Subsequently, we obtain a very large effective axion-coupling term $\vartheta$ at the resonance frequency (Supplementary Fig. 8). Hence the demonstrated Tellegen metamaterial provides a promising platform for exploring axion-related physics. Here we would like to note that, due to the presence of spatial dispersion in the metamaterial, the retrieved parameters under normal incidence would not rigorously explain the electromagnetic responses at oblique incidence with significant incident angles.

### Near-field characterization

We further study the magnetoelectric response of the Tellegen metamaterial via near-field characterization at its surface on the transmission side. Figure 4 shows the $E_z$ component of the nearfield distributions on an *x*-*y* plane at the transmission side of the sample where the circular metal coils are indicated by the dashed circles. At the frequency of 8.7 GHz, which is away from the resonance frequency, the Tellegen coupling is negligible (Fig. 3e), and the incident field $E_y$ predominantly excites the electric current in the SRRs oriented in the *y*-direction, inducing charge accumulation and consequently electric dipoles oscillating in the *y*-direction. At the resonance frequency of 9.5 GHz, the strong Tellegen coupling of the metamaterial induces the electric dipole oscillating in the *x*-direction. As a result, the superposition of the electric dipoles oscillating in the *y*-direction and *x*-direction leads to an overall nearfield oscillating at a tilted angle with respect to the *y*-axis (Fig. 4b). At a higher frequency of 10.2 GHz, beyond the resonance frequency, the Tellegen coupling starts to vanish, leading to a nearfield $E_z$ predominantly oscillating in the *y* direction (Fig. 4c). The measured near-field distribution is shown in the lower panels of Fig. 4, showing good agreement with the simulated results. Therefore, the microscopic probing of the magnetoelectric nearfield provides further evidence of the Tellegen response. Interestingly, despite that the electric dipoles oscillating at a tilted angle close to the resonance frequency, the transmission should preserve the same polarization as the incident wave, which is protected by the combination of the inversion symmetry and Onsager–Casimir relations (Supplementary Materials Section 6). However, lacking any symmetry protection, the polarization of reflected wave is changed as a result of nonreciprocal interaction of incident wave with the metamaterial.

## Discussion

In summary, we have proposed and experimentally demonstrated a metamaterial slab that exhibits a pure Tellegen response. Such a Tellegen metamaterial is constructed by assembling resonant metallic coils, YIG rods and permanent magnets in a judicious manner, such that the Tellegen response is dramatically enhanced and meanwhile other bianisotropic effects are canceled. By measuring both the co- and

cross-polarized reflection and transmission, we observe a giant polarization rotation in reflection, with a Kerr rotation reaching 90° at the resonance frequency. Meanwhile, the transmission wave remains the same polarization as the incident wave, characteristic of a pure Tellegen response. The extracted effective Tellegen coupling term is several orders of magnitude larger than that of natural materials. Our study bridges the gap in the experimental realization of Tellegen metamaterial, which has significant implications for the understanding of nonreciprocal magnetoelectric response and holds promise for various applications like electromagnetic isolators and nonreciprocal twist polarizers. Furthermore, the Tellegen metamaterial assumes particular importance in the realm of fundamental physics, unlocking the potential for experimental exploration of intriguing and exotic concepts of axion electrodynamics.

## Methods

### Simulation

We simulated the transmission and reflection spectra of the device using the commercial software COMSOL Multiphysics based on the finite element method (FEM). The relative permeability tensor of the gyromagnetic materials has the form $\tilde{\mu}=\begin{bmatrix}\mu_r & i\kappa & 0\\ -i\kappa & \mu_r & 0\\ 0 & 0 & 1\end{bmatrix}$, where $\mu_r=1+\frac{(\omega_0+i\alpha\omega)\omega_m}{(\omega_0+i\alpha\omega)^2-\omega^2}$, $\kappa=\frac{\omega\omega_m}{(\omega_0+i\alpha\omega)^2-\omega^2}$, $\omega_m=4\pi\gamma M_s$, $\omega_0=\gamma\mu_0 H_0$, and $\mu_0 H_0$ is the external magnetic field along the z direction which is considered as 0.22 T, $\gamma=2.8$ MHz/Oe is the gyromagnetic ratio, $\alpha=0.002$ is the damping coefficient, and $\omega$ is the operating frequency. The saturation magnetization has been set to $4\pi\gamma M_s=1780$ Oe. Non-zero insertion loss is used in the simulation (PCB material) to match the practical experiment. Since the metasurface is periodic, we simulate a single unit cell with periodic boundary condition.

### Experimental setups

To measure the near-field, we employ a horn antenna acting as a source and a dipole antenna acting as a probe to receive electromagnetic waves, which is placed 0.5 mm above the samples. The transmission measurement is performed in the microwave regime using two horn antennas (operational range 8–15 GHz) to sweep the frequency. In order to minimize the Fabry-Pérot effect between slab and antenna in the direction of transmission and reflection, the measured signal in frequency domain was transformed into time domain. Then we use time gating to isolate a single response in space to alleviate the interference pattern presented in frequency domain.

## Data availability

Data supporting key conclusions are available in the main text and the Supplementary materials. Data that support all other findings of this study are available from the corresponding author upon request.

## References


1. Tellegen, B. D. The gyrator, a new electric network element. *Philips Res. Rep.* **3**, 81–101 (1948).
2. Post, E. & Seeger, R. J. Formal structure of electromagnetics. *Am. J. Phys.* **33**, 597 (1965).
3. Serdyukov, A., Semchenko, I., Tretyakov, S. & Sihvola, A. Electromagnetics of bi-anisotropic materials: Theory and applications. (Gordon and Breach Science Publishers, United States, 2001).
4. Sihvola, A. H. Are nonreciprocal bi-isotropic media forbidden indeed? *IEEE Trans. Microw. Theory Tech.* **43**, 2160–2162 (1995).
5. Sihvola, A. H., Tretyakov, S. A., Serdyukov, A. N. & Semchenko, I. V. Duality once more applied to Tellegen media. *Electromagnetics* **17**, 205–211 (1997).
6. Sochava, A. A., Simovski C. R. & Tretyakov, S. A. Electromagnetic waves in a material with simultaneous mirror-conjugated and racemic chirality characteristics. *Electromagnetics* **20**, 481–488 (2000).
7. Tretyakov, S., Sochava, A., Khaliullin, D. Y. & Yatsenko, V. Artificial nonreciprocal uniaxial magnetoelectric composites. *Micro. Opt. Tech. Let.* **15**, 260–263 (1997).
8. Asadchy, V. S., Díaz-Rubio, A. & Tretyakov, S. A. Bianisotropic metasurfaces: Physics and applications. *Nanophotonics-Berl.* **7**, 1069–1094 (2018).
9. Liu, L. X. et al. Broadband metasurfaces with simultaneous control of phase and amplitude. *Adv. Mater.* **26**, 5031–5036 (2014).
10. Tse, W.-K. & MacDonald, A. H. Giant magneto-optical Kerr effect and universal Faraday effect in thin-film topological insulators. *Phys. Rev. Lett.* **105**, 057401 (2010).
11. Banzer, P., Wozniak, P., Mick, U., De Leon, I. & Boyd, R. W. Chiral optical response of planar and symmetric nanotrimers enabled by heteromaterial selection. *Nat. Commun.* **7**, 13117 (2016).
12. Semchenko, I., Khakhomov, S. & Samofalov, A. Optimal helix shape: Equality of dielectric, magnetic, and chiral susceptibilities. *Russian Phys. J.* **52**, 472–479 (2009).
13. Guo, Q. H. et al. Observation of three-dimensional photonic dirac points and spin-polarized surface arcs. *Phys. Rev. Lett.* **122**, 203903 (2019).
14. Niemi, T., Karilainen, A. O. & Tretyakov, S. A. Synthesis of polarization transformers. *IEEE T Antenn Propag.* **61**, 3102–3111 (2013).
15. Ra'Di, Y., Asadchy, V. S. & Tretyakov, S. A. Total absorption of electromagnetic waves in ultimately thin layers. *IEEE T Antenn Propag.* **61**, 4606–4614 (2013).
16. Hehl, F. W., Obukhov, Y. N., Rivera, J.-P. & Schmid, H. Relativistic nature of a magnetoelectric modulus of Cr 2 O 3 crystals: A four-dimensional pseudoscalar and its measurement. *Phys. Rev. A* **77**, 022106 (2008).
17. Qi, X.-L., Hughes, T. L. & Zhang, S.-C. Topological field theory of time-reversal invariant insulators. *Phys. Rev. B* **78**, 195424 (2008).
18. Wu, L. et al. Quantized Faraday and Kerr rotation and axion electrodynamics of a 3D topological insulator. *Science* **354**, 1124–1127 (2016).
19. Feng, J. L. Dark matter candidates from particle physics and methods of detection. *Annu. Rev. Astron. Astrophys.* **48**, 495–545 (2010).
20. Nenno, D. M., Garcia, C. A. C., Gooth, J., Felser, C. & Narang, P. Axion physics in condensed-matter systems. *Nat. Rev. Phys.* **2**, 682–696 (2020).
21. Sekine, A. & Nomura, K. Axion electrodynamics in topological materials. *J. Appl. Phys.* **129**, 141101 (2021).
22. Astrov, D. Magnetoelectric effect in chromium oxide. *Sov. Phys. JETP* **13**, 729–733 (1961).
23. Gao, A. Y. et al. Layer Hall effect in a 2D topological axion antiferromagnet. *Nature* **595**, 521 (2021).
24. Zhang, D. Q. et al. Topological axion states in the magnetic insulator MnBi2Te4 with the quantized magnetoelectric effect. *Phys. Rev. Lett.* **122**, 206401 (2019).
25. Coh, S. & Vanderbilt, D. Canonical magnetic insulators with isotropic magnetoelectric coupling (vol 88, 121106, 2013). *Phys. Rev. B* **90**, 159903 (2014).
26. Mong, R. S. K., Essin, A. M. & Moore, J. E. Antiferromagnetic topological insulators. *Phys. Rev. B* **81**, 245209 (2010).
27. Li, R. D., Wang, J., Qi, X. L. & Zhang, S. C. Dynamical axion field in topological magnetic insulators. *Nat. Phys.* **6**, 284–288 (2010).
28. Liu, F., Xu, J. & Yang, Y. Polarization conversion of reflected electromagnetic wave from topological insulator. *JOSA B* **31**, 735–741 (2014).
29. Prudêncio, F. R., Matos, S. A. & Paiva, C. R. Asymmetric band diagrams in photonic crystals with a spontaneous nonreciprocal response. *Phys. Rev. A* **91**, 063821 (2015).
30. Wilczek, F. Two applications of axion electrodynamics. *Phys. Rev. Lett.* **58**, 1799 (1987).

31. Kamenetskii, E., Sigalov, M. & Shavit, R. Tellegen particles and magnetoelectric metamaterials. *J. Appl. Phys*. **105**, 013537 (2009).
32. Prudêncio, F. R. & Silveirinha, M. G. Synthetic axion response with space-time crystals. *Phys. Rev. Appl*. **19**, 024031 (2023).
33. Safaei Jazi, S. et al. Optical Tellegen metamaterial with spontaneous magnetization. *Nat. Commun*. **15**, 1293 (2024).
34. Seidov, T. Z. & Gorlach, M. A. Hybridization of electric and magnetic responses in the effective axion background. *Phys. Rev. A* **108**, 053515 (2023).
35. Shaposhnikov, L., Mazanov, M., Bobylev, D. A., Wilczek, F. & Gorlach, M. A. Emergent axion response in multilayered metamaterials. *Phys. Rev. B* **108**, 115101 (2023).
36. Tretyakov, S. A. et al. Artificial tellegen particle. *Electromagnetics* **23**, 665–680 (2003).
37. Kamenetskii, E. O., Awai, I. & Saha, A. K. Experimental evidence for magnetoelectric coupling in a ferromagnetic resonator with a surface metallization. *Micro. Opt. Tech. Let*. **24**, 56–60 (2000).
38. Devescovi, C. et al. Axion topology in photonic crystal domain walls. *Nat Commun* **15** (2024).
39. Yang, Q. D., Chen, W. J., Chen, Y. T. & Liu, W. Electromagnetic duality protected scattering properties of nonmagnetic particles. *Acs Photonics* **7**, 1830–1838 (2020).
40. Tretyakov, S. A. Electromagnetics of complex media - chiral, biisotropic and bianisotropic materials. *Radiotekh Elektro*. **39**, 1457–1470 (1994).
41. Ra'di, Y. & Grbic, A. Magnet-free nonreciprocal bianisotropic metasurfaces. *Phys. Rev. B* **94**, 195432 (2016).
42. Mirmoosa, M., Ra'di, Y., Asadchy, V., Simovski, C. & Tretyakov, S. Polarizabilities of nonreciprocal bianisotropic particles. *Phys. Rev. Appl* **1**, 034005 (2014).
43. Ra'di, Y., Asadchy, V. & Tretyakov, S. One-way transparent sheets. *Phys. Rev. B* **89**, 075109 (2014).
44. Yang, Q. D., Chen, W. J., Chen, Y. T. & Liu, W. Ideal Kerker scattering by homogeneous spheres: The role of gain or loss. *Beilstein J. Nanotech* **13**, 828–835 (2022).
45. Jaggard, D., Mickelson, A. & Papas, C. On electromagnetic waves in chiral media. *Appl. Phys*. **18**, 211–216 (1979).
46. Zhang, S. et al. Negative refractive index in chiral metamaterials. *Phys. Rev. Lett*. **102**, 023901 (2009).
47. Zhang, S., Liu, F., Zentgraf, T. & Li, J. S. Interference-induced asymmetric transmission through a monolayer of anisotropic chiral metamolecules. *Phys. Rev. A* **88**, 023823 (2013).
48. Kong, J. A. Theory of electromagnetic waves (Wiley-Interscience, New York, 1975).
49. Prudencio, F. R., Matos, S. A. & Paiva, C. R. Asymmetric band diagrams in photonic crystals with a spontaneous nonreciprocal response. *Phys. Rev. A* **91**, 063821 (2015).
50. Park, A. J., Pfeiffer, C. C., Chabanov, A. A. & Grbic, A. in *2024 IEEE International Workshop on Antenna Technology (iWAT)*. 43-46.
51. Liu, N. et al. Giant nonreciprocal transmission in low-biased gyrotropic metasurfaces. *Opt. Lett*. **45**, 5917–5920 (2020).
52. Fisanov, V. V. Reflection of plane waves from an impedance boundary in a non-reciprocal bi-isotropic tellegen medium. *Russian Phys. J*. **56**, 562–569 (2013).


## Acknowledgements

This work was supported by the New Cornerstone Science Foundation, the Research Grants Council of Hong Kong (AoE/P-502/20, STG3/E-704/23-N, 17309021), Guangdong Provincial Quantum Science Strategic Initiative (GDZX2204004, GDZX2304001).

## Author contributions

S.Z. conceived the idea and guided the project. Q.D.Y. performed numerical simulations. Q.D.Y., X.H.W., Z.F.L. and O.B.Y. performed theoretical analysis. Q.D.Y. conducted the experiments under the supervision of S.Z.. Q.D.Y. and Z.F.L. processed the experimental data. Q.D.Y., W.X.H. and Z.F.L. analyzed the experimental results. Q.D.Y. and W.X.H. wrote the manuscript with input from all authors. All authors contributed to the discussion.

## Competing interests

The authors declare no competing interests.

## Additional information

**Supplementary information** The online version contains supplementary material available at https://doi.org/10.1038/s41467-024-55159-0.

**Correspondence** and requests for materials should be addressed to Shuang Zhang.

**Peer review information** *Nature Communications* thanks the anonymous reviewer(s) for their contribution to the peer review of this work. A peer review file is available.